Thermodynamic Assessment of Water Absorption For Subsea CO_2 Separation in Offshore Blue Ammonia Production Concepts for Brazilian Pre-Salt

Anderson Rapello dos Santos [a,b,c], Fábio Alves Albuquerque [d], Cláudia Honnicke[d], Marcos Coradini Tolfo[a], Hamza Alhamad [e], Carine Menezes Rebello[e], Erbet Almeida Costa[e], Robson Pessoa[e], Idelfonso Nogueira[e], Cédric Guyon[b], Frèdèric Rousseau[b] and Florian Pradelle[c]

[a] Petróleo Brasileiro S.A. (PETROBRAS), Rio de Janeiro, RJ, Brasil,
anderson.r.santos@petrobras.com.br (CA)
[b] École Nationale Supérieure de Chimie de Paris, Chimie Paris Tech, Paris, France
[c] Pontifical Catholic University of Rio de Janeiro (PUC-Rio), Department of Mechanical Engineering, (DEM) and Institute for Mobility and Sustainable Energy (IMES), Rio de Janeiro, RJ, Brazil
[d] Petróleo Brasileiro S.A. (PETROBRAS), R&D Centre, CENPES, Rio de Janeiro, RJ, Brasil
[e] Norwegian University of Science and Technology (NTNU) / Department of Chemical Engineering

Abstract:

Several offshore blue ammonia production concepts based on Floating Production, Storage and Offloading (FPSO) units have received Approval in Principle (AiP) from certification agencies, reflecting the successful adaptation of mature onshore technologies to offshore environments for the monetization of associated natural gas from adjacent installations. However, the deployment of these concepts in Brazilian pre-salt fields remains strongly constrained by the high CO_2 content of the produced gas and by the energy-intensive nature of the CO_2 separation stages required both for feed stream conditioning and for the recompression of gas directed to Enhanced Oil Recovery (EOR) applications. In this context, subsea separation emerges as a technically attractive alternative by exploiting the naturally favorable high-pressure and low-temperature conditions of the subsea environment. This work evaluates the thermodynamic potential of CO_2 absorption in water as a mechanism for early CO_2 separation in offshore blue ammonia production concepts, through a direct comparison with membrane-based separation using Aspen HYSYS. The analysis is carried out based on steady-state simulations of two hybrid subsea-topside architectures associated with FPSO units, incorporating CO_2 separation stages based on physical absorption of CO_2 in water and on membrane separation, respectively. Particular attention is given to the impact of pressure losses induced by the separation processes and to the resulting recompression requirements for CO_2 streams intended for EOR. The thermodynamic behavior of multicomponent CH_4-CO_2 mixtures is described using the Peng-Robinson equation of state, with heavy hydrocarbons represented by four pseudocomponents. System performance is assessed through energy and exergy analyses, enabling the quantification of energy demand, exergy destruction, and overall efficiencies associated with each separation alternative. The results indicate that CO_2 absorption in water under subsea conditions reduce the topside compression demand up to 50% and reduce the associated exergy destruction during gas conditioning, resulting in measurable improvements in both energy and exergy efficiencies when compared to membrane-based separation and representing an improvement of up to 140% in hydrocarbon recovery per unit of energy supplied. Overall, the findings corroborate the potential of CO_2 absorption in water as a technically robust and energy-efficient pathway for early CO_2 separation in low-carbon offshore blue ammonia production systems.

Keywords:

Thermodynamics; Energy; Exergy; Subsea Processing; Blue Ammonia.

1. Introduction

The transition toward low-carbon energy systems has intensified efforts to decarbonize energy-intensive value chains through technological pathways that simultaneously address energy security, economic performance, and sustained greenhouse-gas (GHG) abatement. In this context, ammonia produced from fossil feedstocks integrated with carbon capture and storage (CCS), commonly referred to as blue ammonia, has gained prominence as both a strategic hydrogen carrier and a tradable commodity in industrial and energy markets

[1]. In parallel, advances in subsea processing enable selective CO_2 removal at seabed conditions, reducing gas throughput to topside facilities and improving conditions for CO_2 reinjection and enhanced oil recovery (EOR). Subsea separation systems operating under supercritical or dense-phase conditions are particularly attractive because they can mitigate thermodynamic irreversibilities associated with gas transport and topside processing, especially in hybrid architectures linking seabed pre-processing with low-carbon hydrogen and ammonia production [2,3]. In Brazil, Petrobras has accumulated extensive experience in subsea system deployment, including the development of HISEP™, which performs high-pressure multiphase separation of CO_2-rich production streams on the seabed and significantly reduces topside processing demand. However, subsea CH_4–CO_2 separation remains technically challenging. Membrane-based or permeation-dominated systems introduce pressure losses that require repressurization, particularly for CO_2 streams destined for reinjection, thereby increasing compression duty and thermodynamic irreversibilities and potentially offsetting part of the benefits of early separation [4–6]. This motivates the evaluation of subsea separation technologies specifically designed to minimize pressure losses and recompression requirements.

Accordingly, the present work evaluates integrated concepts for offshore blue ammonia production from pre-salt natural gas by comparing three gas-conditioning pathways: (i) low-pressure-loss subsea CO_2 separation under supercritical conditions, (ii) subsea membrane-based separation, and (iii) conventional topside gas processing. The analysis combines steady-state HYSYS™ simulations, equation-of-state-based thermodynamic modeling for CH_4–CO_2 mixtures, and energy and exergy assessments. Emphasis is placed on compression demand and pressure-loss penalties, since these directly affect energy consumption, operating expenditure, and downstream recompression requirements. The results provide quantitative indicators to support early-stage concept selection and reinforce the importance of integrated thermodynamic evaluation frameworks linking process performance, emissions behavior, and system-level costs in complex offshore environments. The remainder of the paper presents the system definition and modeling assumptions, the methodological framework, the simulation and statistical results, and the main conclusions.

2. Process Modelling Definitions

2.1. Process Modelling

The system analyzed in this study corresponds to an integrated offshore production architecture designed to process 180,000 barrels of oil per day, 16 million m³/day of natural gas, and 10 million Sm³/day of CO_2 for CCUS and EOR, with part of the produced gas routed to an ammonia synthesis unit. Three processing configurations are evaluated. Figure 1 presents a simplified schematic of the evaluated process configurations. The first is a conventional FPSO-based scheme including three-stage separation, free-water knockout, flash separation, and CO_2-CH_4 separation, followed by CO_2 recompression for reinjection and natural-gas export. This configuration is treated as the base case, consistent with Santos et al. [3]. The second and third correspond to low-TRL hybrid subsea separation concepts, in which High-Pressure Gas-Liquid Separation (HISEP™) is combined with downstream separation of the dense CO_2-CH_4 phase via either (i) subsea membrane modules or (ii) subsea liquid-liquid extraction. In both alternatives, gas conditioning occurs upstream of the FPSO, with the objective of reducing topside footprint, compression duty, and overall energy demand, while enabling dense-phase CO_2 reinjection.

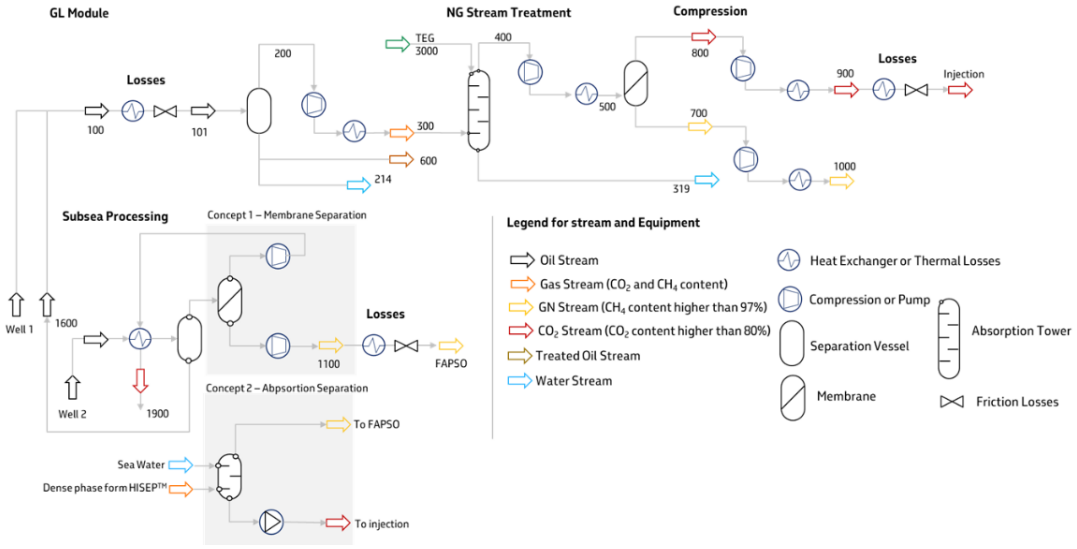

Figure. 1. *Process representation for concepts assessed in this study.*

These benefits, however, are accompanied by increased technological complexity and operability risks typical of subsea separation systems. The process model was developed in Aspen HYSYS™ v15 based on mass and energy-balance principles and integrates both subsea and topside processing units under operating conditions representative of the PPSBS. Flowlines and subsea layout elements were excluded from the scope. The inlet stream undergoes pressure reduction to 17 bar for three-phase separation, followed by oil expansion to 4.5 bar to promote gas disengagement, with associated gas streams subsequently recompressed and combined prior to CO_2-CH_4 separation. The subsea separation module assumes a multiphase oil feed at 150 bar and 100 °C with CO_2 molar fractions up to 57%. Dense-phase separation leverages the thermodynamic behaviour of PPSBS fluids, allowing two or occasionally three coexisting liquid phases and enabling gravitational removal of an immiscible CO_2-rich phase. The hydrocarbon-rich liquid phase (<25 mol% CO_2) is routed to topside treatment, whereas the dense CO_2-rich phase is cooled, recompressed to 150 bar, and reinjected for EOR, with optional blending of surface-treated streams following Zanetti [7].

Phase equilibrium calculations were performed using an isothermal flash formulation. For a specified temperature T [K], pressure P [bar], total molar feed flow rate F [kg/h], and overall composition z, the model simultaneously solves for vapor and liquid phase fractions (V/F and L/F) and their respective compositions (y_i and x_i). These $2N-2$ unknowns are obtained by solving a corresponding system of nonlinear equations expressing thermodynamic equilibrium, as detailed in Eq. (1) to (4):

$$F = L + V \Leftrightarrow z_i F = x_i L + y_i V, \sum_{i=1}^{N} x_i - \sum_{i=1}^{N} y_i = 0, \ \frac{y_i}{x_i} = \frac{\hat{\phi}_i^l(T,P,x_i)}{\hat{\phi}_i^v(T,P,y_i)} \tag{1}$$

Liquid-liquid (L-L) separation is treated analogously, by enforcing the equality of component fugacities in the two coexisting liquid phases α and β, in an equation-of-state framework.

$$f_i^{\alpha}(T,P,x^{\alpha}) = f_i^{\beta}(T,P,x^{\beta}) \ , \ \hat{\phi}_i^{\alpha}(T,P,x^{\alpha})x_i^{\alpha} = \hat{\phi}_i^{\beta}(T,P,x^{\beta})x_i^{\beta} \tag{2}$$

subject to the overall and component mass balances:

$$F = L^{\alpha} + L^{\beta} \Longrightarrow F z_i = x_i^{\alpha} L^{\alpha} + x_i^{\beta} L^{\beta} \tag{3}$$

$$\sum_{i=1}^{N} x_i^{\alpha} - \sum_{i=1}^{N} x_i^{\beta} = 0 \tag{4}$$

The numerical algorithm solves the above equations in a unified flash-calculation framework, allowing identification of single-phase, V-L, L-L, or V-L-L conditions depending on pressure, temperature and overall composition. Despite known limitations in supercritical regions, the PR-EoS was adopted due to its robustness and widespread use for hydrocarbon systems according to Eq. (5) described by Peng et al. [11]:

$$P = \frac{RT}{V-b} - \frac{a}{V(V+b)+b(V-b)} \tag{5}$$

Parameter a is an energy dependent on temperature and composition, while b represents the co-volume, which is a function of composition only. These parameters can be defined using an appropriate mixing rule, such as the quadratic mixing rule, which also includes the binary interaction parameter k_{ij} according to Eq. (6) and (7) according as Peng, et al., [12].

$$a = \sum_i \sum_j x_i x_j (a_i a_j)^{1/2} (1 - k_{ij}) \tag{6}$$

$$b = \sum_i x_i b_i \tag{7}$$

Heat exchangers were modelled via energy balances and fluid thermodynamic properties. The cooler employed a simplified approach using global heat-transfer coefficients, whereas the reheater, used for thermal integration, was modelled with the Logarithmic Mean Temperature Difference (LMTD) method, according to Souza (2018). The heat duty Q represents the rate of thermal energy transfer between the two fluids in the heat exchanger, expressed in MW. The overall heat-transfer coefficient U accounts for all thermal resistances in series, including convective heat transfer on both fluid sides, conductive resistance through the wall, and any fouling layers, and is expressed in $\mathrm{W\,m^{-2}\,K^{-1}}$. The heat-transfer area A corresponds to the effective surface available for heat exchange between the fluids, measured in $\mathrm{m^2}$. Where Logarithmic Mean Temperature Difference (LMTD) is given by Eq. (8) for counter current flow.

$$Q = UA\Delta T_{ln} \ , \Delta T_{ln} = \frac{\Delta T_1 - \Delta T_2}{ln\left(\frac{\Delta T_1}{\Delta T_2}\right)}, \ T_1 = T_{h,in} - T_{c,out} \ \Delta T_2 = T_{h,out} - T_{c,in} \tag{8}$$

The membrane mass transport modelling requires the application of the component-wise mass conservation equation, which enables the prediction of process performance and the optimization of operating conditions. In this study, a proprietary plugin was implemented in the Aspen HYSYS™ v15 platform to simulate the membrane separation process according to Souza (2024). The permeance of each component k was represented according to Eq. (9), allowing the quantitative evaluation of mass transfer rates and selectivity under varying operating conditions.

$$N_k = \Pi_k A_{MP} \left[\frac{\left(P_v^{out} y_k^{out} - P_l^{out} x_k^{out}\right) - \left(P_v^{in} y_k^{in}\right)}{ln\left(\frac{P_v^{out} y_k^{out} - P_l^{out} x_k^{out}}{P_v^{in} y_k^{in}}\right)} \right] \tag{9}$$

The molar flux of component k, N_k, represents the rate at which species k is transported across the membrane per unit time, driven by the partial-pressure difference between vapor and liquid streams. The parameter $\Pi_k$denotes the membrane permeability (or permeance) of component k, capturing both the intrinsic transport properties of the membrane material and its effective thickness. The term A_{MP} corresponds to the effective membrane contact area available for mass transfer. The driving force for permeation is expressed in terms of the logarithmic mean partial-pressure difference of component k across the membrane module. Here, P_v^{in} and P_v^{out} denote the total vapor-phase pressures at the membrane inlet and outlet, respectively, while y_k^{in} and y_k^{out} are the corresponding vapor-phase mole fractions of component k. Similarly, P_l^{out} and x_k^{out} correspond to the liquid-phase pressure and mole fraction of component $k$at the membrane outlet. The terms $(P_v y_k)$ and $(P_l x_k)$ therefore represent the partial pressures of component $k$in the vapor and liquid phases. The use of the logarithmic means accounts for the spatial variation of the driving force along the membrane path, ensuring thermodynamic consistency when evaluating mass transport under non-uniform conditions. The performance of the CO_2-CH_4 liquid-liquid separation system was quantified using four key performance indicators. The CO_2-CH_4 selectivity reflects the relative preference of the solvent (or CO_2-rich phase) for CO_2 compared with CH_4, and is defined as Eq. (10):

$$S_{CO_2-CH_4} = \frac{\left(x_{CO_2}^E \Big/ x_{CO_2}^R\right)}{\left(x_{CH_4}^E \Big/ x_{CH_4}^R\right)} \tag{10}$$

where x_i^E and x_i^F denote the mole fractions of component $i$in the extract (CO_2-rich) and feed stream, respectively. The CO_2 recovery to the extract phase is given by Eq. (11):

$$R_{CO_2} = \frac{\dot{n}_{CO_2}^E}{\dot{n}_{CO_2}^F} \tag{11}$$

where $\dot{n}_{CO_2}^E$and $\dot{n}_{CO_2}^F$are the molar flow rates of CO_2 in the extract and feed streams. Conversely, the CH_4 loss to the CO_2-rich phase is defined as Eq. (12):

$$L_{CH_4} = \frac{\dot{n}_{CH_4}^E}{\dot{n}_{CH_4}^F} \tag{12}$$

representing the fraction of CH_4 undesirably entrained in the extract. Finally, to compare the two different process alternatives on a consistent energetic basis, an energy-normalized recovery index is defined as Eq. (13):

$$R_{CO_2}^* = \frac{R_{CO_2}}{\sum_i^n \dot{W}_{sep}} \tag{13}$$

where $\dot{W}_{sep}$ in MW is the separation power demand. Together, these indicators provide a comprehensive description of thermodynamic selectivity, mass partitioning performance, and energy-efficiency trade-offs relevant to dense-phase CO_2 separation and conditioning upstream of the FPSO. Table 1 outlines the conditions of the feed stream, sourced from reservoir.

Table 1 *- Feed stream Well 1 and Well 2 properties for HYSYS™ simulation.*

Property	Value	Unit	Component molar fraction	Scenario			
				1	2	3	4
Vapor Fraction	0.845	-	H_2O	0.0500	0.0500	0.1000	0.1707
Subsea processing inlet T	90	°C	CO_2	0.3000	0.5000	0.5000	0.5000
Subsea processing inlet P	150	bar	CH_4	0.5002	0.3463	0.3078	0.2534
Molar Flow	13,053	kmol/h	F_1	0.0724	0.0501	0.0445	0.0367
Mass Flow	735,317	kg/h	F_2	0.0077	0.0053	0.0047	0.0039
Mass Enthalpy	935.4	kcal/kg	F_3	0.0385	0.0266	0.0237	0.0019
Std Ideal Liquid Volumetric Flow	1,105	m^3/h	F_4	0.0311	0.0215	0.0192	0.0158

2.1. Fluid Characterization

The reservoir fluid was modeled based on a Brazilian dead light oil, as characterized by Lucas et al. [8], to represent the composition of pre-salt reservoir oil. The crude oil was fractionated into four distinct fractions with pseudo-components (F_1 to F_4). These fractions were then blended with CH_4, CO_2, and H_2O in proportions consistent with those observed in the original dead oil, resulting in a hypothetical reservoir fluid. The simulations were carried out using the commercial software HYSYS™ and, as described in detail in Souza et al. [7], Peng-Robinson equation of state (EOS-PR) is used to model the fluid behavior. The binary interaction parameters (BIPs) k_{ij} between the oil fractions and CO_2 were derived by Lucas et al. [8] through the fitting of experimental phase equilibrium data to the PR-EOS predictions. BIPs for other components, including CH_4, were sourced from Souza [9] and Souza et al. [10]. Interactions between hydrocarbons were deemed negligible due to their minimal influence. The properties critical temperature and pressure, accentric factor, molecular weight, fugacity factor for water and CO_2 associated with the EOS-PR model are provided in Table 2.

Table 2. *Binary interaction parameters (BIP), for EOS-PR as Lucas, et al. [8].*

Species	Standard Chemical Exergy (kJ/mol)	T_c (ºC)	P_c (bar)	ω	MW (g/mol)	$k_{i,H2O}$	$k_{i,CO2}$
H_2O	3.12E+03	374	220.6	0.344	18.0	-	0.2
CO_2	2.01E+04	31	73.7	0.293	44.0	0.2	-
CH_4	8.37E+05	-82.6	46.0	0.011	16.0	0.5	0.105
F_1	5.44E+06	335.2	27.9	0.161	117.7	0.5	0.0906
F_2	7.40E+06	386.7	22.7	0.478	160.9	0.5	0.0790
F_3	1.07E+07	495.6	18.8	0.551	231.1	0.5	0.0960
F_4	1.16E+07	622.5	12.1	0.865	447.6	0.5	0.0960

2.3. Thermodynamic Analysis

The efficiency of a thermodynamic process is defined as the ratio between the useful energy rate, provided by the streams Well 1 and Well 2 from the reservoir, according to Figure 1, in term of higher heating value (HHV_i) of the outputs (stream 600 for export oil, stream 1000 and 1900 for export gas and stream 800 and 1800 for CO2-CH4 injection) and the total supplied energy to the processing unit, based on the first law of thermodynamics according to Eq. (14), considering heat rate $\dot{Q}$ [MW], power $\dot{W}_s$ [MW], and mass flow for each component i $\dot{m}_i$ [kg/s].

$$\eta_{HHV} = \frac{\dot{E}_{out}}{\dot{E}_{in}} = \frac{\sum_{i=1}^{n} \dot{m}_{i,out} \cdot HHV_{i,out}}{\sum_{i=1}^{n} \dot{m}_{i,in} \cdot HHV_{i,in} + \dot{Q} + \dot{W}_s} \quad (14)$$

Similarly, the efficiency can also be written on an enthalpy basis, where only the thermal enthalpy content of the process streams is considered. In this case, the enthalpy-based efficiency is defined by Eq. (15) as:

$$\eta_{enthalpy} = \frac{\dot{E}_{out}}{\dot{E}_{in}} = \frac{\sum_{i=1}^{n} \dot{m}_{i,out} \cdot h_{i,out}}{\sum_{i=1}^{n} \dot{m}_{i,in} \cdot h_{i,in} + \dot{Q} + \dot{W}_s} \quad (15)$$

where $h_{i,in}$ is specific enthalpy of stream i in [kJ/kg] and the numerator represents the total enthalpy rate of the outlet streams and the denominator accounts for the enthalpy rate of the inlet streams, supplemented by external heat supply and ancillary energy consumption. It is important to note that, unlike HHV-based efficiency definitions, the enthalpy formulation does not include the chemical energy associated with fuel oxidation, but only the enthalpy referenced to a defined thermodynamic state. The exergy rate of each stream [MW] can be defined as the sum of physical exergy rate ($\dot{E}_{ph}$), given in Eq. (16) and the specific chemical exergy ($\dot{E}_{ph}$), given in Eq. (17). The chemical exergy of the stream was defined as the sum of the standard chemical exergy of its components determined under reference conditions of T_0 = 298 K and P_0 = 1 bar, used by Kotas [11], minus the compression work (only for gas stream).

$$\dot{E}_{ph} = \sum_{i=1}^{n} m_i\left[\left(h_i + h_{i,o}\right) - T_o\left(s_i - s_{i,o}\right)\right] \quad (16)$$

$$\dot{E}_{ch} = \dot{N}\left(\sum_{i=1}^{n} x_i e_{ch_{i,o}} + RT_o \sum_{i(gas)=1}^{n} x_i ln(x_i)\right) \quad (17)$$

where T_0, h_0, and s_0 represent the reference temperature [K], specific enthalpy [kJ/kg], and specific entropy [kJ/kg.K], respectively. The specific enthalpy and entropy for each control volume in the streams are indicated by h and s, respectively, with index i. The exergy rate associated with power ($\dot{E}_{xW}$) is the proper power, while the exergy rate ($\dot{E}_{xq}$) associated with the rate of heat transfer ($\dot{Q}$) is given according to Eq. (18) with all terms given in MW, where T0 represents the reference temperature, and Tr is the temperature at the system boundary, estimated as the average temperature between the inlet and outlet streams in [K].

$$\dot{E}_{xq} = \dot{Q}\left(1 - \frac{T_o}{T_r}\right) \quad (18)$$

By incorporating the exergy rate of both the inlet ($\dot{E}_{x,in}$) and the outlet ($\dot{E}_{x,out}$) of the control volume, the overall exergy balance is expressed in Eq. (19).

$$\dot{E}_{x,in} = \dot{E}_{x,out} + \dot{E}_{xd} = \dot{E}_{xp} + \dot{E}_{xl} + \dot{E}_{xd} \quad (19)$$

where $\dot{E}_{xp}$ represents the exergy rate of useful products, $\dot{E}_{xl}$ represents the exergy rate of losses, corresponding to the exergy rate associated with mass or energy flows discharged to the environment, and $\dot{E}_{xd}$ is the rate of exergy destruction, all expressed in MW. Thus, exergy efficiency, according to Eq. (20), was employed to assess the proposed processing alternatives, defined as the ratio of the exergy rate of the useful product ($\dot{E}_{xp}$) to the exergy rate of the inlet ($\dot{E}_{x,in}$), both expressed in MW.

$$\varepsilon = \frac{\dot{E}xp}{\dot{E}_{x,in}} = 1 - \frac{\dot{E}xd + \dot{E}xl}{\dot{E}_{x,in}}, \varepsilon = \frac{\dot{E}x_{out}}{\dot{E}x_{in}} = \frac{\sum_{i=1}^{n} \dot{m}_{i,out} \cdot \dot{e}x_{i,out}}{\sum_{i=1}^{n} \dot{m}_{i,in} \cdot \dot{e}x_{i,in} + \dot{Q} + \dot{E}xl} \quad (20)$$

In this context, the exergetic efficiency of the separation system was evaluated according to the definition proposed by Tsatsaronis [12], in which the useful exergy contained in the product streams is compared with the total exergy supplied to the system. In the present analysis, the useful product streams were defined as those with predominantly hydrocarbon composition, since the objective is to compare the thermodynamic performance of two alternative subsea CO_2-separation processes while preserving the exergy associated with the recoverable natural-gas fraction. This definition differs from the approach adopted by Santos et al. [4], in which the CO_2-rich stream is also treated as a useful product due to its potential for indirect monetization when employed for Enhanced Oil Recovery (EOR). Accordingly, the total useful exergy was obtained as the sum of the physical and chemical exergy contributions of the hydrocarbon-rich streams. The exergetic efficiency (ε) was then calculated as the ratio between the useful exergy and the total input exergy, with all exergy rates expressed in megawatts [MW]. By explicitly defining the streams considered in the calculation of the overall exergetic efficiency, including both the exergy supplied to the system and the useful exergy associated with the product streams, the global process exergetic efficiency can be written in the form presented in Eq. (21), which accounts for the physical and chemical exergy contributions of each relevant stream presented in Figure 1.

$$\varepsilon = \frac{\left(\dot{E}_{ch_{600}} + \dot{E}_{ph_{600}}\right) + \left(\dot{E}_{ch_{1000}} + \dot{E}_{ph_{1000}}\right) + \left(\dot{E}_{ch_{1900}} + \dot{E}_{ph_{1900}}\right)}{\sum_{i=1}^{2}\left(\dot{E}_{ch_{Well\,1}} + \dot{E}_{ph_{Well}}\right)_i + \sum_{i}^{n} \dot{E}_{HEx} + \sum_{i}^{n}\left(\dot{E}_{Pumps} + \dot{E}_{Comp}\right)} \quad (21)$$

3. Methodology

The methodological framework adopted in this work consisted of three main stages. First, the alternative gas-conditioning concepts were defined, and the operating scenarios were selected to be representative of the field lifetime, with systematic variation of CO_2 content, gas-oil ratio (GOR), and feed flow rate. For each scenario, the thermodynamic performance was quantified through the response functions defined in Eq. (17), (18) and (23), while CO_2-separation selectivity, CH_4-loss performance and energy-normalized recovery index were evaluated according to Eq. (13), (14) and (16). Figure 2 illustrates the workflow adopted in this study.

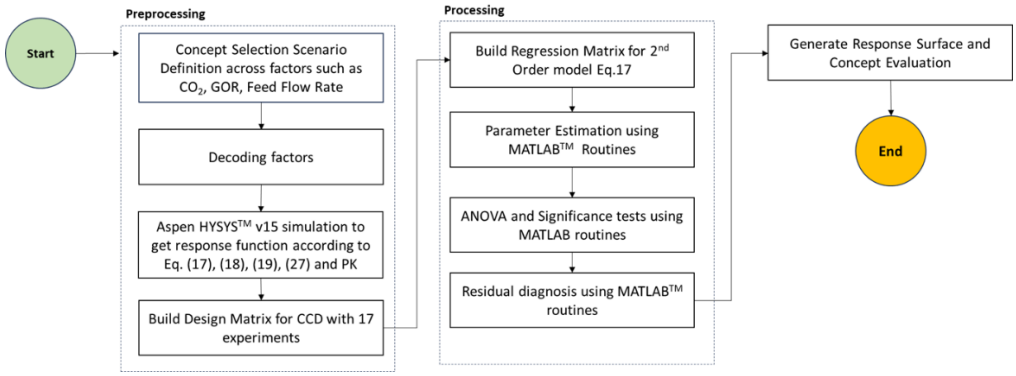

Figure. 2. *Workflow integrating Aspen HYSYS™ process modelling and MATLAB® based statistical analysis.*

The real operating variables were then coded into dimensionless factors and used to construct a Central Composite Design (CCD) comprising 17 experiments, enabling the estimation of second-order response surfaces.The levels were established based on representative pre-salt compositions, ranging from for 0.30/0.05 (low CO_2/H_2O), 0.50/0.1 (central point), to 0.70/0.15 (high CO_2/H_2O), complemented by axial (alpha) points to capture non-linear effects, with CO_2 varying from 0.1636 to 0.8364 and H_2O from 0.0159 to 0.1841. The regression coefficients were obtained using the least-squares method, and the statistical robustness of the models was subsequently assessed through ANOVA, following the approach described by Santos et al. (2026), to evaluate model significance and lack of fit. Validated response surfaces were then generated to support the comparative assessment of the processing concepts, allowing the combined influence of CO_2 content, GOR, and feed flow rate on thermodynamic performance, CO_2 selectivity, and methane retention to be systematically quantified. The process models were developed and executed in Aspen HYSYS™ v15, whereas the statistical analysis and response-surface evaluation routines were implemented in MATLAB®.

4. Results and Discussion

4.1. Statistical Model Evaluation and Results

The comparative analysis of the subsea separation concepts, membrane-based and liquid-liquid extraction, was carried out using a CCD comprising 17 experiments. The following response functions were evaluated: the energy efficiency based on the higher heating value (y_1, Eq. (17)), the enthalpy-based efficiency (y_2, Eq. (18)), the exergetic efficiency (y_3, Eq. (25)), the energy-normalized recovery index (y_4, Eq. (16)), the subsea energy demand (y_5), and the topside energy demand (y_6). The independent factors considered were the CO_2 and H_2O molar fractions in the feed gas (x_1 and x_2, respectively). Statistical representativeness of the fitted response-surface models was verified by ANOVA, and coefficients of determination (R^2) above 0.90 were achieved for all response variables in both concepts, except for y_3. For the absorption-based concept, the ANOVA results are summarized in Table 3.

Table 3 *- Design Matrix for CCD and Full Factorial Design, two factors with 17 experiments for Absorption concept.*

Anova	Response Function for Central Composite Design for Absorption Concept					
	y_1	y_2	y_3	y_4	y_5	y_6
SS for model	0.10	0.14	0.04	0.00002	123.63	27736.63
SS for residual	0.00	0.00	0.01	0.00001	0.64	517.02
F Test	95.95	370.91	14.41	256.44	577.31	160.94
P Value	0.00001	0.00001	0.0054	0.000001	0.00001	0.00001
R^2	0.96968	0.99198	0.82768	0.98844	0.99483	0.98170

For all response functions, the model sum of squares was substantially larger than the residual sum of squares, indicating good agreement between the quadratic CCD model and the simulated data. The F-test values ranged from 14.41 for the exergetic efficiency (y_3) to 577.31 and 160.94 for the subsea and topside energy-demand functions (y_5 and y_6), respectively, with all corresponding p-values below 10^{-3}. These results confirm the statistical significance of the fitted models at the 95% confidence level. The coefficients of determination R^2 ranged from 0.8277 for y_3 to 0.9948 for y_5, with the remaining responses exhibiting R^2 values above 0.97. Although the exergetic-efficiency model (y_3) presents the lowest determination coefficient among the responses, with $R^2 = 0.83$, it still captures most of the response variability and remains statistically significant.

The comparatively lower R^2reflects the stronger sensitivity of chemical-exergy calculations to phase-equilibrium composition, and, consequently, to the thermodynamic model, which amplifies propagation of uncertainty relative to the purely energy-based metrics. This behavior can be attributed to the intrinsic sensitivity of the chemical-exergy term to the predicted phase-equilibrium compositions. Since the chemical exergy depends explicitly on species fugacities and reference-state deviations, any uncertainty associated with the thermodynamic model used to describe CH_4-CO_2-H_2O non-idealities, particularly under dense-phase and multiphase in supercritical conditions, is amplified when computing the exergetic efficiency. As a result, small deviations in phase composition prediction propagate non-linearly into the chemical-exergy balance, leading to larger dispersion in the exergetic-efficiency response and consequently to a lower R^2 when compared with purely energy-based performance metrics. Table 3 reports the regression coefficients of the response functions in terms of the coded independent variables, namely the molar CO_2 content ($A = x_1$) and the water content ($B = x_2$). The corresponding regression statistics are summarized in Tables 3 to 5. For the subsea absorption concept, the CCD coefficients indicate that CO_2 content (factor A) is the main variable governing system performance. Both the HHV-based and enthalpy-based efficiencies (y_1 and y_2) decrease with increasing CO_2 content, as evidenced by the negative linear coefficients in A, while the small negative linear term in B shows that water content has a weaker adverse effect on performance.

Table 4 *- Summary for Coefficient Assessment for CCD two factors with 17 experiments for Absorption Subsea Concept.*

Coefficient	Response Function for Central Composite Design for Absorption Subsea Separation					
	y_1	y_2	y_3	y_4	y_5	y_6
Intercept	+0.9292	+0.2370	+0.8492	0.0379	26.3503	59.8443
A	-0.0920	-0.1287	-0.0252	0.0062	-3.8057	49.6610
B	-0.0160	-0.0357	-	0.0010	-0.6155	4.72140
A^2	-0.0598	-	-0.0640	0.0021	-0.7517	30.5871
B^2	-	-	-	-	-	3.10230
AB	-	-	-	-	-	-

For the exergetic efficiency (y_3), both the linear and quadratic coefficients in A are negative, indicating that exergy efficiency degrades progressively as CO_2 concentration increases, with curvature becoming more pronounced at higher CO_2 levels. Regarding energy demand, subsea energy consumption (y_5) shows a negative linear dependence on both $A$and B, together with a small negative quadratic term in A^2, confirming only moderate composition sensitivity in the evaluated range. In contrast, topside energy demand (y_6) exhibits strong dependence on CO_2 content through both linear and quadratic contributions, with an additional (though smaller) quadratic dependence on water content. No statistically relevant interaction terms were identified, indicating that CO_2 and H_2O act largely independently. The coefficients confirm that CO_2 molar fraction is the dominant factor, while the influence of water content remains secondary. For the membrane-based concept, the ANOVA results are presented in Table 5. As observed for the absorption system, the model sum of squares is significantly higher than the residual sum of squares for all response functions, indicating good agreement between the quadratic CCD models and the simulated data. The F-test values range from 8.45 for the exergetic efficiency (y_3) to 282.94 for the enthalpy-based efficiency (y_2), with all associated p-values below 10^{-3}, confirming the statistical significance of the models at the 95% confidence level. The determination coefficients R^2 range from 0.738 for y_3 to 0.990 for y_2, while the energy-demand responses (y_5 and y_6) also exhibit high explanatory power, with $R^2 = 0.93$ and 0.98, respectively. Although the exergetic-efficiency model shows the lowest R^2, it still captures most of the variability and remains statistically significant. The ANOVA results demonstrate that the CCD-based polynomial models adequately represent the influence of feed composition on the thermodynamic performance of the membrane-based subsea separation concept.

Table 5 *- Design Matrix for CCD and Full Factorial Design, two factors with 17 experiments for Membrane concept.*

Anova	Response Function for Central Composite Design					
	y_1	y_2	y_3	y_4	y_5	y_6
SS for model	0.07	0.08	0.04	0.01	3985.59	24396.00
SS for residual	0.00	0.00	0.02	0.00001	293.29	574.89
F Test	79.24	282.94	8.45	70.51	40.77	160.94
P Value	0.00001	0.00001	0.00176	0.000001	0.00001	0.00001
R^2	0.96352	0.98951	0.73798	0.95919	0.93146	0.97698
Coefficient						
Intercept	+0.9067	+0.2189	+0.8454	0.0172	58.0028	59.6636
A	-0.0796	-0.0994	-0.0554	0.0183	-10.6166	46.8764

B	-0.0154	-0.0245	-	-	-	-
A^2	-0.0477	-	-0.0427	0.0185	-19.0778	28.1089
B^2	-	-	-	-	-	-
AB	-	-	-	-	-	-

For the membrane-based configuration, the CCD coefficients in Table 6 indicate that CO_2 content (factor A) is again the dominant factor influencing system performance. Both HHV and enthalpy-based efficiencies (y_1 and y_2) decrease with increasing CO_2 content, as reflected by the negative linear coefficients in A, while the smaller negative coefficients associated with Bshow that water content has a weaker adverse effect on efficiency. The exergetic-efficiency response (y_3) is governed by a combination of linear and quadratic CO_2 effects, indicating a progressive deterioration in exergy efficiency as CO_2 concentration rises, with curvature becoming more relevant at higher CO_2 fractions. For y_4, the positive linear and quadratic coefficients in Aindicate a direct and increasingly nonlinear dependence of this indicator on CO_2 content. In contrast, subsea energy demand (y_5) exhibits strong negative linear and quadratic dependence on CO_2, meaning that higher CO_2 levels reduce the specific subsea energy consumption within the design domain. Topside energy demand (y_6) shows substantial linear and quadratic dependence on CO_2, confirming that compression-related duties are highly sensitive to feed composition. No statistically relevant interaction terms between $A$and Bwere identified, suggesting largely independent effects of CO_2 and H_2O. The coefficient assessment confirms that CO_2 molar fraction is the primary driver of efficiency and energy-demand behavior, while water content exerts only secondary influence in the membrane-based subsea separation process.

4.2. Thermodynamic Evaluation Results

Table 6 summarizes the thermodynamic and energy-performance indicators for the four operating scenarios defined in Table 1. Overall, the absorption-based subsea separation concept consistently outperforms the membrane-based configuration in terms of thermal efficiency, subsea power demand, and energy-normalized recovery, while both systems present broadly similar exergetic efficiencies. For all scenarios, the enthalpy and HHV-based efficiencies remain higher for the absorption process, with the difference becoming more pronounced as the CO_2 fraction increases and methane content decreases. Exergy efficiencies remain high for both systems (≈0.83-0.98), although the membrane concept exhibits slightly lower values in Scenarios 2-4, indicating higher irreversibilities under CO_2-rich conditions. A key differentiating factor is the subsea energy requirement. The membrane-based configuration demands between 42-60 MW across the scenarios, whereas the absorption concept requires only 25-30 MW, evidencing a substantially lower energetic penalty at the seabed. Topside power demand is comparable between concepts and follows the expected trend of increasing with CO_2 and H_2O content. Exergy destruction increases significantly with methane dilution for both concepts, reaching 1.2-1.3 GW in the most severe case, and shows no systematic bias toward either technology. Finally, the energy-normalized recovery index is consistently higher for the absorption process, indicating superior hydrocarbon recovery per unit of energy supplied. In contrast, the membrane concept yields lower recovery productivity, reflecting the combined effect of higher energy consumption and hydrocarbon losses. In summary, within the composition envelope defined in Table 1, the subsea absorption concept exhibits a clear energetic advantage over the membrane-based alternative.

Table 6 *–Consolidated Performance Indicators Subsea Concepts Evaluation.*

Indicator		Unit	Membrane Subsea Concept				Absorption Subsea Concept			
			Scenarios							
			1	2	3	4	1	2	3	4
Energy Efficiency	Enthalpy	%	0.9326	0.9153	0.9079	0.8940	0.9511	0.9381	0.9304	0.9173
	HHV		0.3427	0.2544	0.2229	0.1798	0.3823	0.2798	0.2265	0.1946
Exergy Efficiency			0.9812	0.8580	0.8475	0.8273	0.9838	0.8608	0.8468	0.8336
Power Demand	Subsea	MW	42.37	55.98	57.48	59.94	29.65	27.02	26.45	25.52
	Topside		49.33	56.69	59.03	62.92	49.29	57.14	59.22	63.01
Exergy Destruction			192	1241	1260	1290	179	1217	1266	1244
Recovery Normalized		kgmol/h.MW	0.0234	0.0178	0.0173	0.0166	0.0337	0.0370	0.0378	0.0392

This advantage arises primarily from its substantially lower subsea power demand and higher energy-normalized recovery for the separation models evaluated, while the exergetic-efficiency levels remain broadly comparable between the two concepts. Figure 2 shows the contour maps of the energetic efficiencies for the membrane concept, obtained using the coefficients reported in Table 5 and calculated from (a) the higher

heating value (HHV), (b) the enthalpies of the inlet and outlet streams, and (c) the exergetic efficiency. In this case, the exergetic efficiency is predominantly governed by the chemical exergy of the mixture, which is mainly associated with its hydrocarbon content. Since CO_2 and H_2O contribute negligibly to the chemical-exergy term and act essentially as inert diluents, the simultaneous increase in their molar fractions during field depletion leads to a marked reduction in the thermodynamic quality of the gas stream. This behavior results in the minimum exergetic efficiency observed in the contour map, where the combined presence of elevated CO_2 and H_2O concentrations amplifies exergy destruction by mixing and separation, yielding the poorest exergetic performance of the membrane system within this operating region. In contrast to the membrane-based separation, the absorption process exhibits an opposite trend with respect to feed composition.

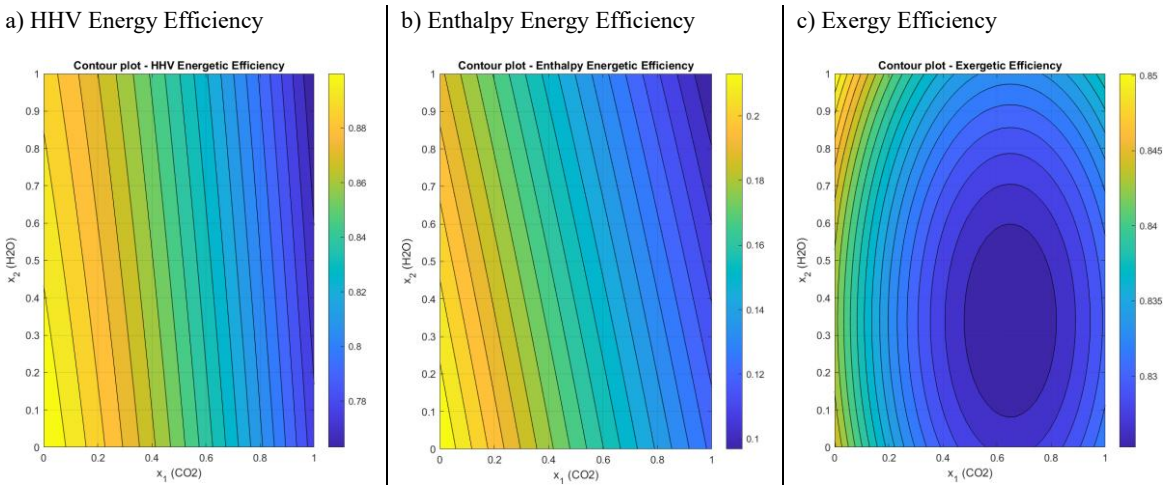

Figure. 3. *Contour maps of energetic and exergetic efficiencies for the membrane-based separation process.*

As shown in Figure 4, the exergetic efficiency increases with increasing CO_2 molar fraction in the feed gas. This behavior is associated with the intrinsically selective nature of the absorption process, in which CO_2 is the preferentially absorbed species. Higher CO_2 concentrations enhance the chemical driving force for mass transfer and allow the process to operate closer to a thermodynamically reversible regime, thereby reducing irreversibilities associated with mixing and separation. In addition, the removal of hydrocarbons from the gas stream becomes less significant at elevated CO_2 contents, which limits the loss of chemical exergy linked to the fuel fraction. As a result, the absorption process attains its highest exergetic efficiencies under CO_2-rich conditions, in clear contrast with the membrane system, where the combined presence of CO_2 and H_2O leads to a minimum in exergetic performance.

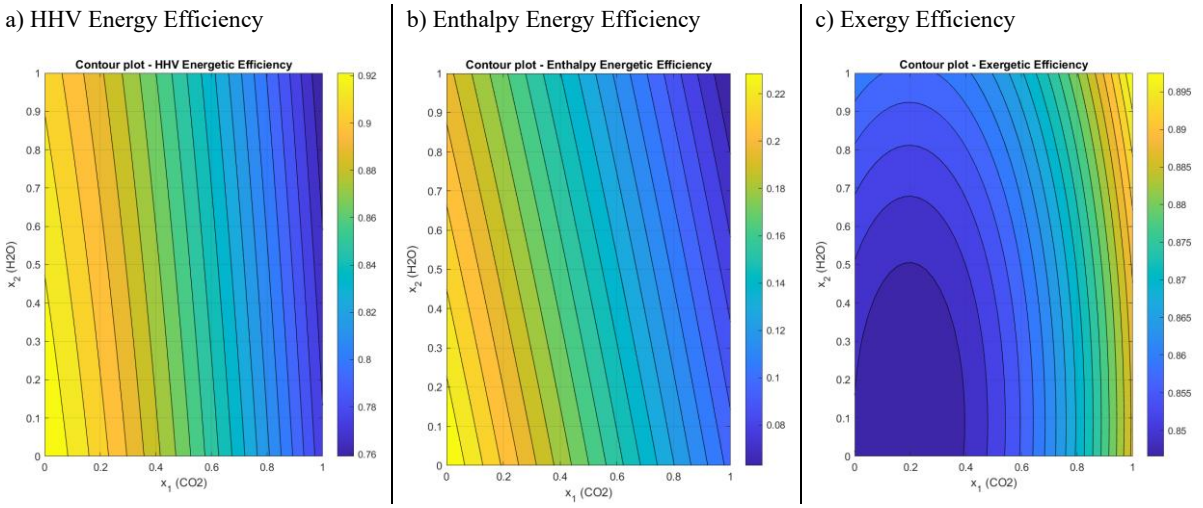

Figure. 4. *Contour maps of energetic and exergetic efficiencies for the membrane-based separation process.*

A comparative assessment of the response variable y_5 for the absorption- and membrane-based CO_2 separation concepts, combined with the exergetic analysis, reveals clear differences in the way both processes respond to variations in feed-gas composition. For the absorption system, the contour and 3D-surface maps

show a smooth and nearly linear decrease in $y_5$with increasing CO_2 molar fraction, with only a weak dependence on the H_2O content.

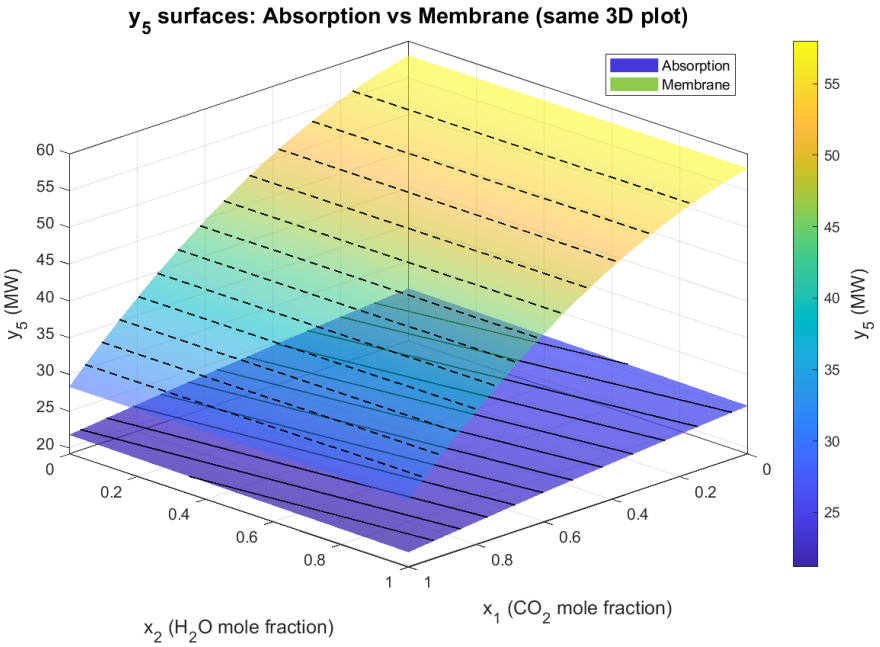

Figure. 5. *Subsea power demand comparison between absorption and membrane concepts.*

This trend is fully consistent with the exergetic efficiency maps, where the absorption process exhibited improved performance under CO_2-rich conditions. In thermodynamic terms, this behaviour reflects the intrinsically selective nature of the absorption route, which increasingly favours CO_2 removal as its concentration rises, thereby reducing irreversibilities associated with mixing and separation. In contrast, the membrane process displays a substantially higher baseline value of y_5 together with a much stronger and highly non-linear dependence on the CO_2 fraction, as reflected by the steep gradients and pronounced curvature observed in both the contour and 3D-surface plots. This behaviour is aligned with the exergetic analysis, which identified a region of minimum exergetic efficiency for the membrane concept at elevated CO_2 and H_2O levels, indicating significant thermodynamic penalties under these compositions. Overall, the combined exergetic and $y_5$analyses demonstrate that the absorption route is composition-robust and benefits from CO_2 enrichment, whereas the membrane route is considerably more sensitive to feed composition and may operate under strongly unfavourable exergetic conditions in specific regions of the operating space.The combined energetic, exergetic and response-surface analyses consistently indicate that the subsea absorption-based separation concept offers a more favorable and robust thermodynamic performance envelope than the membrane-based alternative over the range of gas compositions evaluated. In addition to presenting systematically lower subsea power demand and higher energy-normalized recovery, the absorption route exhibits a smooth and nearly linear improvement in performance as the CO_2 molar fraction increases. This trend is fully consistent with the exergetic efficiency maps, which show that absorption increasingly favors CO_2 removal under CO_2-rich conditions, thereby reducing irreversibilities associated with mixing and phase separation. By contrast, the membrane-based concept displays a significantly higher baseline power requirement and a strongly non-linear dependence on feed-gas composition, including a well-defined region of minimum exergetic efficiency at elevated CO_2 and H_2O contents. Although the absolute difference in subsea power demand between the two concepts does not increase monotonically with CO_2 enrichment, due to the progressive reduction of the energetic content of the feed stream, normalization of this difference by the available methane fraction reveals a pronounced increase in the relative energetic penalty of membrane separation under advanced field-depletion scenarios. This behaviour is primarily driven by the intrinsic pressure losses of the permeation process and the associated recompression requirements for CO_2 reinjection, which amplify thermodynamic irreversibilities as the hydrocarbon fraction decreases. While the present work is limited to a comparative thermodynamic assessment, these results consistently demonstrate the superior thermodynamic robustness and compositional resilience of absorption-based separation for subsea CO_2 management in pre-salt developments across the full production life cycle.

5. Conclusions

This work presented a comparative thermodynamic assessment of two subsea CO_2 separation concepts, membrane permeation and solvent absorption, under representative pre-salt gas compositions. A design-of-experiments framework was applied to quantify the sensitivity of energy and exergy efficiencies, as well as energy-demand indicators, to variations in CO_2 and H_2O content, reflecting the expected compositional evolution over the field life cycle. The results show that the absorption-based concept systematically outperforms the membrane system, with clear and quantifiable energetic advantages. Subsea power demand is reduced from 42–60 MW to 25–30 MW, corresponding to a reduction of approximately 30–55%. This translates into significantly higher energy-normalized recovery, increasing from 0.0166–0.0234 $kgmol \cdot h^{-1} \cdot MW^{-1}$ for membranes to 0.0337–0.0392 $kgmol \cdot h^{-1} \cdot MW^{-1}$ for absorption, representing improvements of up to 140%. In addition, the absorption process consistently exhibits higher HHV-based efficiencies, particularly under CO_2-rich conditions, while both technologies maintain comparable exergetic efficiencies (0.83–0.98). These results indicate that, despite similar thermodynamic limits, absorption achieves superior energy utilization by reducing mechanical losses associated with pressure drops and recompression. From a compositional perspective, absorption performance improves with increasing CO_2 content due to enhanced mass-transfer driving forces and reduced irreversibilities. In contrast, the membrane process shows a strongly non-linear response, including a region of minimum exergetic efficiency at high CO_2 and H_2O levels, where exergy destruction reaches up to ~1.3 GW. Overall, the absorption route demonstrates greater thermodynamic robustness and compositional resilience, particularly under advanced field-depletion conditions. Although limited to thermodynamic analysis, the magnitude and consistency of these differences support the preferential consideration of absorption-based subsea CO_2 separation for pre-salt developments. Nevertheless, practical implementation will depend on addressing key operational challenges, including solvent management, equipment reliability, process control, and long-term subsea operability. Future work should focus on improving thermophysical modeling under supercritical conditions, validating the concepts with experimental and field data, extending exergoeconomic analyses, and assessing the integration of subsea CO_2 separation with offshore blue-ammonia production systems.

6. Acknowledgements

The authors acknowledge the institutional support of the Pontifical Catholic University of Rio de Janeiro (PUC-Rio). This work was also supported by the Brazilian Coordination for the Improvement of Higher Education Personnel (CAPES), Funding Code 001. The authors would like to thank the CNPq for the Bolsa de Produtividade em Pesquisa (PQ; grant number: 308627/2025-3) and the FAPERJ for Jovem Cientista do Nosso Estado (JCNE; grant number: E-26/204.488/2025) grants awarded to Florian Pradelle.

7. References

[1] Rubin, E.S., Antes, M., Yeh, S., Berkenpas, M. “Estimating the Future Trends in the Cost of CO_2 Capture Technologies.” IEAGHG Report 2006-06, 2006.

[2] Santos, A.R., Roberto, M.A.R., Miller, F., Freire, L.A., Silva, D.F.C., Rebello, M.L.C., Guyon, C., Rousseau, F., Pradelle, F. “Energy, Exergy and Economic Analysis of Subsea Processing for Blue Ammonia Production in Pre-Salt Offshore Operations.” ECOS 2025 Conference Proceedings, Paris, 2025.

[3] Santos, A.R., Alahmad, H., Albuquerque, F.A., Roberto, M.A.R., Honnicke, C.G., Rebello, M.L.C., Nogueira, I.B.R., Guyon, C., Rousseau, F., Pradelle, F. “Thermodynamic Evaluation of Hybrid Offshore Production Systems Integrating Subsea CH_4/CO_2 Separation and Blue Ammonia Synthesis: A DOE-Based Approach.” 18th International Heat Transfer Conference Proceedings, Rio de Janeiro, 2026, under submission.

[4] Augustus, M.R., Dias e Silva, J.C., Koelln, H.P., Bernardes, A.C., Albuquerque, F.A., Paternost, G.M., Oliveira, A.M., Xavier, G.M., da Silva, J.A.G., da Costa, O.C. “Boosting to Boosting: A New Approach to Enhance, Support and Maximize Subsea Processing and Boosting Applications.” Offshore Technology Conference Proceedings, Houston, 2023.

[5] Albuquerque, F.A., Morais, M.G., Euphemio, M.L., Kuchpil, C., Duarte, D.G., Orlowski. “Subsea Processing and Boosting in Brazil: Status and Future Vision.” Offshore Technology Conference Proceedings, Rio de Janeiro, 2013.

[6] Lucas, M.A., Borges, G.R., da Rocha, I.C. “Use of Real Crude Oil Fractions to Describe the High-Pressure Phase Behavior of Crude Oil in Carbon Dioxide.” The Journal of Supercritical Fluids, 118, pp. 14–147, 2016.

[7] Souza, A.F.F. “Separação Submarina Óleo e CO_2: Concepção Tecnológica, Modelagem e Controle Avançado.” M.Sc. Dissertation, Departamento de Engenharia Química, Rio de Janeiro, 2018. [8] Souza, A.F.F., Secchi, A.R., Souza Jr., M.B. “CO_2 Subsea Separation: Concept and Control Strategies.” IFAC Conference Proceedings, 2019.

[9] Peng, D.-Y., Robinson, D.B. “A New Two-Constant Equation of State.” Ind. Eng. Chem. Fundam., 15(1), pp. 59–64, 1976.

[10] Souza, I.R. “Development of the Unit Operation Gas-Liquid Contactor with Membrane in the HYSYS 8.8 Simulator.” M.Sc. Dissertation, Escola de Química, Universidade Federal do Rio de Janeiro, 2024.

[11] Kotas, T.J. The Exergy Method of Thermal Plant Analysis. 1st ed., Anchor Brendon, UK, 1985.

[12] Tsatsaronis, G. Thermoeconomic Analysis and Optimization of Energy Systems. Progress in Energy and Combustion Science, 19, pp. 227–257, 1993.

[13] Zanetti, A., “Produção de Hidrogênio em Unidade Offshore Integrada à Recuperação Avançada de Petróleo: Uma Análise Técnico Econômica.” M.Sc. Dissertation, Escola de Química Universidade Federal do Rio de Janeiro, (2024).

[14] National Petroleum Agency (ANP). Oil and Gas Statistical Yearbook — Brazil 2024. Available at: https://www.gov.br/anp.

[15] Goulart, M.P., Mattoso, M.P. “Buzios FPSO Experience: Standardization and Perspectives for Our Next Generation of Pre-Salt FPSOs.” Offshore Technology Conference Proceedings, Houston, 2021.

[16] Santos, A.R., Alahmad, H., Rebello, M.L.C., Nogueira, I.B.R., Guyon, C., Rousseau, F., Pradelle, F. “Thermodynamic and Economic Performance Assessment of Offshore Blue NH_3 Systems With Early Subsea CO_2 Removal.” 18th International Heat Transfer Conference Proceedings, Rio de Janeiro, 2026, under submission.